Inter-annual variation of lake ice composition in European Arctic: observations based on high-resolution thermistor strings

Bin Cheng[1*], Yubing Cheng[2,3,1*], Timo Vihma[1], Anna Kontu[1], Fei Zheng[2], Juha Lemmetyinen[1,5], Yubao Qiu[4,5] and Jouni Pulliainen[1]

[1] Finnish Meteorological Institute (FMI), Helsinki, Finland

[2] Institute of Atmospheric Physics, Chinese Academy of Sciences, Beijing, China

[3] University of Chinese Academy of Sciences, Beijing, China

[4] Aerospace information Research Institute (AIR), Chinese Academy of Science, Beijing China

[5] FMI-AIR, Joint Research Center for Arctic Observations, Sodankylä, Finland.

*corresponding authors:

Bin Cheng (bin.cheng@fmi.fi)

Yubing Cheng (chengyubing@mail.iap.ac.cn)

Abstract

Climate change and global warming strongly impact the cryosphere. The rise of air temperature and change of precipitation patterns lead to dramatic responses of snow and ice heat and mass balance. Sustainable field observations on lake air-snow-ice-water temperature regime have been carried out in Lake Orajärvi in the vicinity of the Finnish Space Centre, a Flagship Supersite in Sodankylä in Finnish Lapland since 2009. A thermistor string-based snow and ice mass balance buoy called "Snow and ice mass balance apparatus (SIMBA)" was deployed in the lake at the beginning of each ice season. In this paper, we describe snow and ice temperature regimes, snow depth, ice thickness, and ice compositions retrieved from SIMBA observations as well as meteorological variables based on high-quality observations at the Finnish Space Centre. Ice thickness in Lake Orajärvi showed an increasing trend. During the decade of data collection: 1) The November-May mean air temperature had an increasing trend of 0.16º C/year, and the interannual variations were highly correlated (r = 0.93) with the total seasonal accumulated precipitation; 2) The maximum granular ice thickness

ranged from 15 to 80% of the maximum total ice thickness; 3) The snow depth on lake ice was not correlated (r = 0.21) with the total precipitation. The data set can be applied to investigate the lake ice surface heat balance and the role of snow on lake ice mass balance, and to improve the parameterization of snow to ice transformation in snow/ice models. The data are archived at https://zenodo.org/record/4559368#.YIKOOpAzZPZ (Cheng et al., 2021)

1. Introduction

The rapid climate warming in the Arctic (Box et al., 2019; Przybylak and Wyszyński, 2020) has also affected lakes, in particular lake surface temperatures and lake ice phenology (Woolway, et al., 2019). In the Northern Hemisphere, the lake ice season has become shorter and lake ice has become thinner, and these trends are projected to continue throughout the 21st century (Sharma, et al., 2019). Lakes are important in the Earth system, as they can adjust local climate (Brown and Duguay, 2010), and affect the environment through interactions among physical, hydrological, biological, and chemical processes (Leppäranta, 2010).

Observations on snow depth and lake ice thickness are needed for (a) monitoring of climate variability and trends (Filazzola et al., 2020), (b) practical applications, such as use of lake ice for winter fishing, transport, and recreational activities (Leppäranta, 2015), and (c) to provide initial conditions for operational forecasting (Anderson et al., 2018). Snow depth and lake ice thickness can be measured manually. For example, in Finland, lake ice thickness is measured via manual drilling in a single location in 45 lakes with ten-day intervals throughout the ice season. However, this requires a lot of manpower, and accordingly does not allow collection of time series with a better spatial and temporal resolution. During recent decades, the number manual observations has strongly declined in many countries (Duguay et al., 2006). Satellite remote sensing yields information on lake ice cover (Wu et al., 2021) and snow/ice surface temperature (Cheng et al., 2014) with a sufficiently high spatial and temporal resolution. Kang et al., (2014) introduced a method to derive lake ice thickness from coarse resolution (~10 km) passive microwave data over large lakes in Canada. However, the transferability of the method to sub-pixel scale lakes has not been investigated. SAR polarimetry has shown some promise in retrieving ice depth over rivers (Mermoz et al., 2013); as fully polarimetric data is not to

date widely available from existing SAR sensors extensive testing and application of the method for lakes is currently lacking.

The SIMBA data set is potentially highly relevant for the development of land applications for planned and existing passive microwave satellite sensors, such as the Copernicus Imaging Microwave Radiometer (CIMR), new Metop multichannel radiometer sensors of EUMETSAT, ESA SMOS, NASA SMAP and Chinese sensors. Due to the inherent coarse resolution of these sensors (tens of kilometers), a key issue is to acquire combined simultaneous data representing various processes in lakes, in addition to surrounding land areas. As such, the SIMBA forms an integral part of the FMI sensor network in Sodankylä.

Thermistor sting-based snow and ice mass balance apparatus (SIMBA) have been applied for more than a decade to measure snow depth, ice thickness and temperature profile from air through snow and ice to water (Jackson et al., 2013). Most of SIMBA have so far been deployed in Polar sea ice (Lei et al., 2018), but also lake ice has been studied (Cheng et al., 2014; Wei et al., 2016). In this paper we describe SIMBA observations from an ongoing program that started in Lake Orajärvi in northern Finland in 2009. Supporting meteorological observations from Finnish Meteorological Institute Arctic Research Centre (FMI-ARC) are also presented. The objectives of the SIMBA program were

- to evaluate the cost-effectiveness of SIMBA buoys in a remote lake environment
- to monitor climate variability and change as reflected in snow depth as well as lake ice thickness and composition
- to investigate (a) atmospheric forcing on lake ice growth and melt, (b) the role of snow on lake ice mass balance via formation of superimposed ice due to refreezing of melt water and rain and formation of snow ice due to flooding under a heavy snow load, and (c) the role of granular ice in lake ice phenology
- to develop better parameterizations of snow-to-ice transformation in numerical snow/ice models.

2 Observation

2.1 Sodankylä supersite

The SIMBA program at Lake Orajärvi is a component of the FMI Sodankylä supersite. The Finnish

Meteorological Institute's Arctic Space Centre (FMI-ARC) in Sodankylä (67.367 °N, 26.629 °E), Finland, is a super-observation site where various Earth observations (upper-air chemistry and physics, atmospheric column measurements, snow and soil hydrology, biosphere-atmosphere interaction) and ground truth measurements for satellite calibration-validation are carried out continuously (Fig.1). The site is equipped with comprehensive *in situ* and remote sensing instrumentation placed in the forests, wetlands and freshwater bodies, which are the main landcover types in the area. In this paper we focus on the cryospheric *in situ* observations of snow cover and lake ice as well as meteorological parameters.

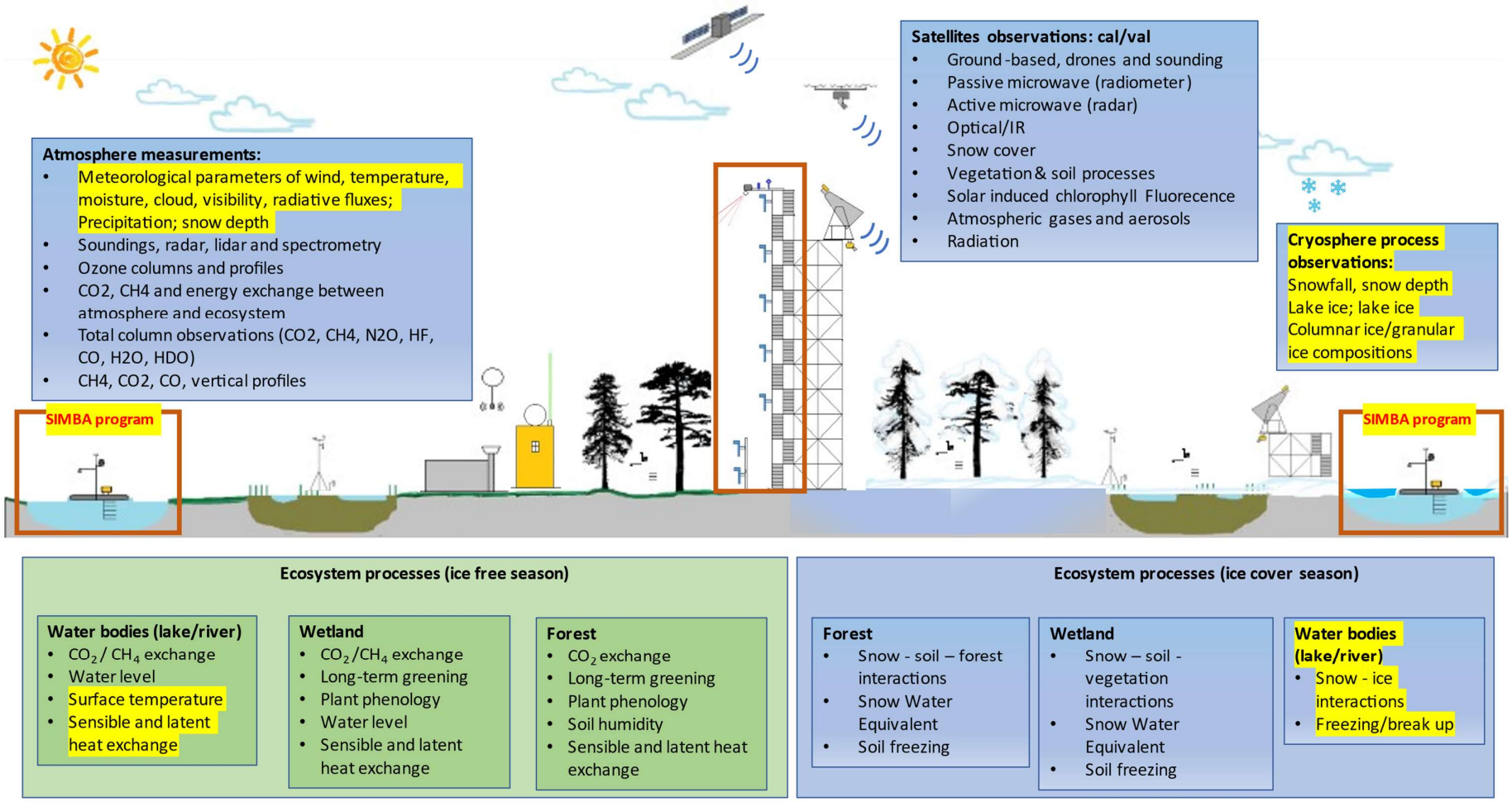

Figure 1. Schematic diagram of the FMI-ARC supersite observational systems at Sodankylä. The original diagram is at https://litdb.fmi.fi/. The frames in red and text with yellow background describes the measurements addressed in this paper.

The sub-Arctic climate and the geographic location between continental and marine climate zones result in a high inter-annual, seasonal and synoptic-scale variation in local weather conditions, enabling development of very different kinds of snowpack structures on land (Tikkanen, 2005) and snow/ice composition on lakes (Cheng et al., 2014). Lake Orajärvi is a boreal medium-sized lake located in Sodankylä municipality in the in the eastern Lapland. The lake has a surface area of about 11 km^2 with an average depth of 4.4 m and a maximum depth of 11 m close to the southern shore of the lake (Fig. 2a). The estimated water volume in the lake is 0.0485 km^3, and the shore length is 28 km. The lake surface elevation is 182 m above sea level. The ice season typically starts in November and lasts until May. The first snowfall typically occurs in late October, but the snow may melt during warmer autumn days. The seasonally permanent winter snow accumulation usually starts between mid-November and early-December. Snow is present on the lake ice surface every winter season.

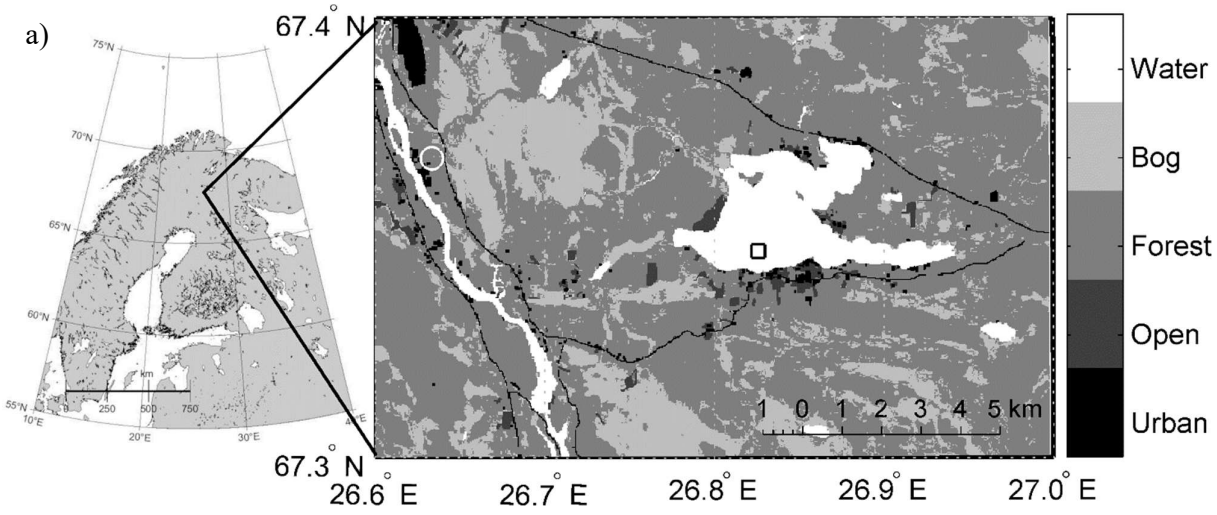

b)

Figure 2. a) The location of Lak Orajärvi in Finnish Lapland and a map of lake Orajärvi and local catchment, where the open black square marks the SIMBA site and white circle is the Finnish Space Centre. b) Snapshots of SIMBA deployment in Lake Orajärvi and a weather station at FMI-ARC main camp. A raft was anchored in the lake in October 2019 aiming to extend the lake observations beyond the ice season.

2.2 SIMBA

2.2.1 SIMBA program

SIMBA buoys have been deployed in Lake Orajärvi since 2009. The 2009 deployment was probably the internationally first SIMBA application for a lake study. In each winter when ice was formed in Lake Orajärvi, one SIMBA was deployed around mid-December at the same site, 67.35º N, 26.83º E, some 500 m from the shoreline. At the time of deployment, the snow depth, lake ice thickness and ice freeboard were measured. A supporting frame made of fiberglass was constructed on lake ice, and the SIMBA main control Peli case was placed on top of it (Fig. 2b). A separate wooden pole with scale was standing vertically to hold the thermistor string. An ice borehole was drilled through the ice layer, and the thermistor string was placed in it. The scene was left as it is, and then the thermistor

string was frozen with surrounding water in the borehole. The SIMBA operated in the lake over the winter and most of the spring melting season. The recovery of SIMBA took place usually in late April but in some years as late as mid-May. Snow and ice conditions around the deployment site were documented and measured before dismantling the SIMBA camp. The documentation on SIMBA deployment and recovery is provided along with the SIMBA data as online files (see data availability). Table 1 summarizes the SIMBA deployment and recovery status.

Table 1. SIMBA deployment and recovery days and simultaneous *in situ* observed snow depth (h_s), total ice thickness (H_i), and ice freeboard (H_{fb}, defined as negative if the lake water level was above the snow/ice interface) The seasonal mean values were derived from SIMBA-ET and SIMBA-HT observations. H_{gi} is the granular ice and H_{ci} is the congelation ice thickness.

Season	Deployment				Recovery					Seasonal mean ± STD				
	Date	h_s	H_i	H_{fb}	Date	h_s	H_{ci}	H_i	H_{fb}	H_i	h_s	H_{sfb}	H_{gi}	H_{ci}
	DD/MM/YY	(cm)			DD/MM/YY	(cm)								
2009/2010	16/12/09	5	27	0	07/04/10	31	54	64	5	NA				
2010/2011	SIMBA was not deployed; only *in situ* observations of h_s,H_i and H_{fb} every second week were available.													
2011/2012	19/12/2011	16	14	-4	12/04/2012	24	22	55	-3	38±16	22±6	5±2	15±10	23±7
2012/2013	12/12/2012	18	33	+1	25/04/2013	0	39	59	6	57±7	26±7	-5±3	4±4	53±4
2013/2014	12/12/2013	14	27	+1	30/04/2014	20	35	35	-3	49±7	17±4	-3±2	10±2	40±6
2014/2015	14/12/2014	19	30	-2.5	23/04/2015	2	35	69	4	54±11	24±7	-4±3	16±8	38±4
2015/2016	18/12/2015	18	27	-1	22/04/2016	5	30	71	6	60±16	19±7	-2±3	12±9	48±9
2016/2017	16/12/2016	8	31	-1	24/04/2017	10	38	72	4	58±13	19±6	-1±2	6±8	50±8
2017/2018	15/12/2017	25	23	-9	03/05/2018	0	28	55	6	48±15	24±6	-4±3	27±14	21±3
2018/2019	13/12/2018	15	19	-2	02/05/2019	1	20	55	6	51±17	21±7	-1±3	21±14	30±7
2019/2020	03/10/2019	-			12/05/2020	4	13	68	7	49±24	24±9	-1±3	32±20	20±5

The seasonal mean values of Hi, h_s, $H_{gi,}$ and H_{ci} were calculated by the SIMBA algorithm (Cheng et al., 2020). The seasonal mean value of ice freeboard (H_{sfb}) was calculated based on time series of snow depth (h_s), granular ice thickness (H_{gi}) and columnar ice thickness (H_i) according to the Archimedes' principle: $H_{sfb} = H_i + H_{gi} - (h_s\rho_s + H_{gi}\rho_{gi} + H_i\rho_i)/\rho_w$, where ρ_s, ρ_{gi}, ρ_i and ρ_w are seasonal mean densities of snow, granular-ice and columnar ice and lake water, assumed to be 320 kg/m^3, 890 kg/m^3 and 910 kg/m^3 and 1000 kg/m^3, respectively. The STD is the standard deviation.

148

149 *2.2.2 SIMBA buoy*

150 SIMBA is a thermistor string-based Snow and Ice Mass Balance Apparatus. It has been developed
151 by the Scottish Association for Marine Science (SAMS) Research Services Ltd (SRSL) in UK.
152 SIMBA consists of a simple, robust thermistor string with 240 temperature sensors distributed evenly
153 (2 cm intervals) along a 4.8 m long heat-shrink PVC plastic sleeve coated flat white wire. White heat-
154 shrink sleeve is used to minimize the possibility of solar heating of the sensors. The accuracy of the
155 SIMBA thermistor sensor is ± 0.1 ºC, which is comparable with other type of thermistor string based
156 IMBs (Richter-Menge et al. 2006). Each sensor measures the environment temperature (SIMBA-ET).
157 The resolution of the thermistor sensor is 0.0625°C, i.e., smaller changes cannot be detected even if
158 the absolute accuracy of the sensor would allow it. In addition, the thermistor chain is equipped with
159 heaters, i.e. resistor components mounted next to the temperature-sensing elements. A weak voltage
160 (8 V) supply is connected to provide gentle identical heating of each sensor on the chain. The SIMBA
161 heating cycle is usually long enough, often 60 or 90 s, for the temperature rise at the sensor to reach
162 a steady state. Thermal conductivity determines how the heat is conducted away of the heated sensors
163 placed in air, snow, ice and lake water. As a result, the SIMBA-HT profiles can greatly enhance the
164 detection of the interfaces between air, snow, ice and water. The heating cycle is applied once per
165 day. The SIMBA-HT is controlled not to disturb the SIMBA-ET measurements which are carried out
166 typically 4 times per day (Jackson et al., 2013). A SIMBA also includes a built-in GPS to record
167 SIMBA drift positions (for sea ice applications), a magnetometer for tilt and floe rotation, a barometer
168 for surface air pressure, and an external sensor to measure near-surface ambient air temperature. An
169 iridium modem is applied for data transmission. SIMBA has been used in various field campaigns
170 targeting snow and ice mass balance in seasonally ice-covers in lakes (Cheng et al., 2014) and Polar
171 Oceans (Hoppmann et al. 2015; Provost et al. 2017; Lei et al. 2018, 2021). Table 1 presents a summary
172 of SIMBA observations in Lake Orajärvi.

173

174 **2.3 Weather station**

175 Meteorological data were collected at FMI-ARC station (67.3666°N, 26.6290°E, WMO code 02836)
176 11 km from Lake Orajärvi. The data sets include wind speed (*Va*), air temperature (*Ta*), relative
177 humidity (*RH*), cloudiness (*cn*), longwave (*Ql*) and shortwave (*Qs*) radiation, snow depth on land (*Hs*)

and precipitation (*Prec*) (Table 2). The radiative fluxes were measured on a 10-m high tower above treetops using Kipp&Zonen CM11 pyranometers (305-2800 nm) and Kipp&Zonen CG4 pyrgeometers (4500 - 42000 nm). Snow depth (Campbell Scientific SR50) and precipitation (OTT Pluvio2) at ground level were also measured. All measurements were taken once a minute and aggregated to 1-hour time intervals.

3 Data description

3.1 SIMBA data

The main output of a SIMBA buoy is the time series of environment (SIMBA-ET) and heating (SIMBA-HT) temperature measured at different depths from the lake water through ice and snow to air.

3.1.1 SIMBA-ET

For each season, we have up to 241 time series of temperature (SIMBA-ET) at different depths. For those sensors located in the air, the temperature differences between the sensors are small, as the air in the lowermost 1.5 m layer mixes effectively and the sensors are close to each other. The temperatures inside snow reveal much larger vertical gradients because snow has a small thermal conductivity. The temperature profile in ice has smaller vertical gradient compared to that in snow, since the thermal conductivity of ice is larger than that of snow. At the ice bottom, temperature is at the freezing point and gradually increases towards the lake bottom. Figure 3 shows an example of seasonal SIMBA-ET. One can estimate the heat fluxes within snow and ice, and those at the air-snow, snow-ice, and ice-water interfaces.

200

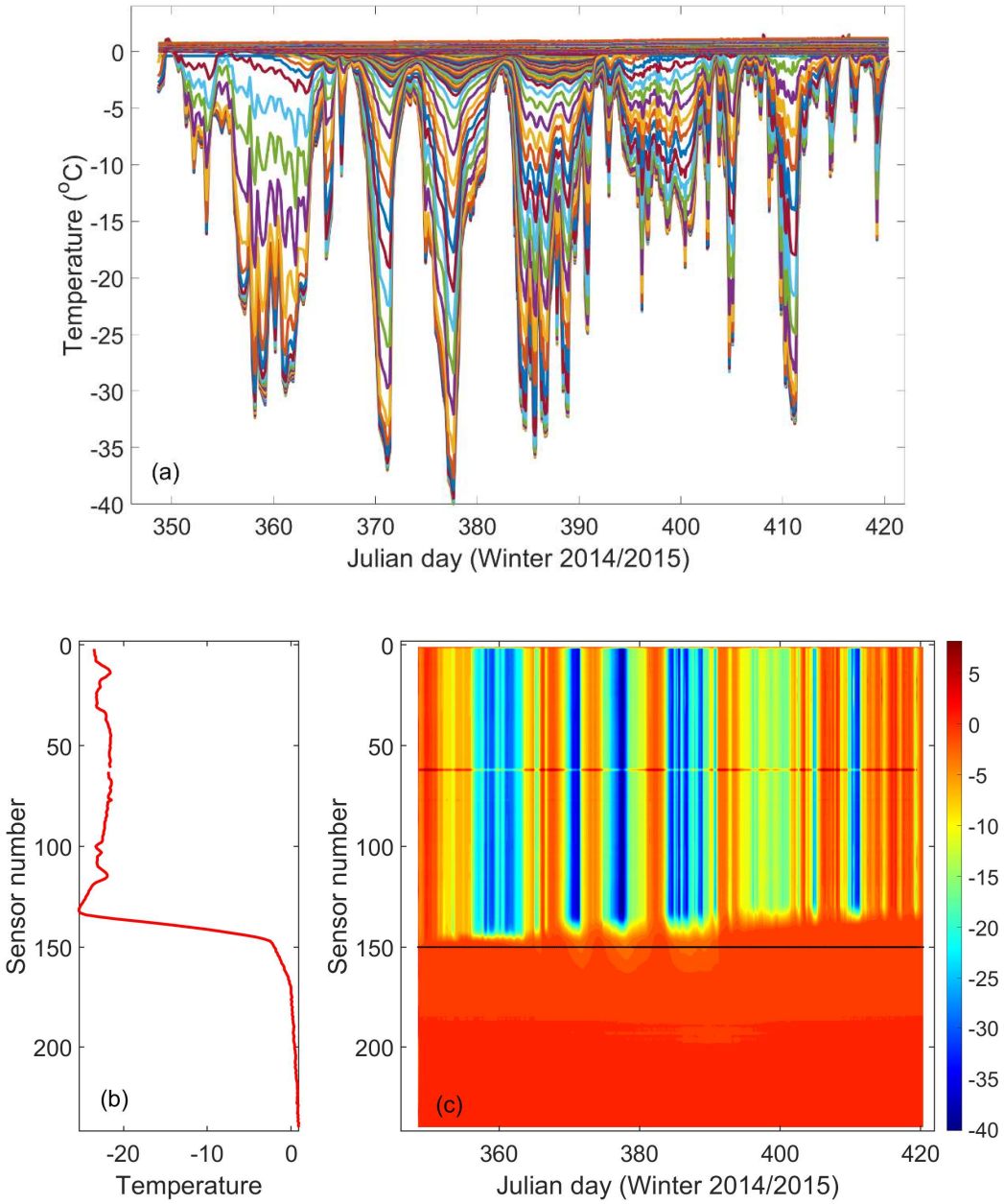

201

202 Figure 3. Illustrations of SIMBA-ET data: a) Time series of SIMBA-ET during observation period;
203 b) One snapshot (19 Jan 2014 08:00 UTC) of vertical SIMBA-ET profile through air-snow-lake ice-
204 water; c) SIMBA-ET field observed by 240 sensors. Sensor 1 was placed in air and sensor 240 in
205 water.

206

207 *3.1.2 SIMBA-HT*

208 SIMBA-HT shows the temperature increase in the medium each sensor was contacted during a short

heating period of 60 s and 90 s. The temperature changes are largely dependent on the thermal diffusivity of the surrounding medium. Low heating power ensures that the temperature increasing will not be too high to melt snow and ice in contact with the sensor and guarantee a fast restore of environment temperature around the sensor before the next SIMBA-ET observation, and above all to minimize SIMBA power consumption. One example of SIMBA-HT is given in Figure 4.

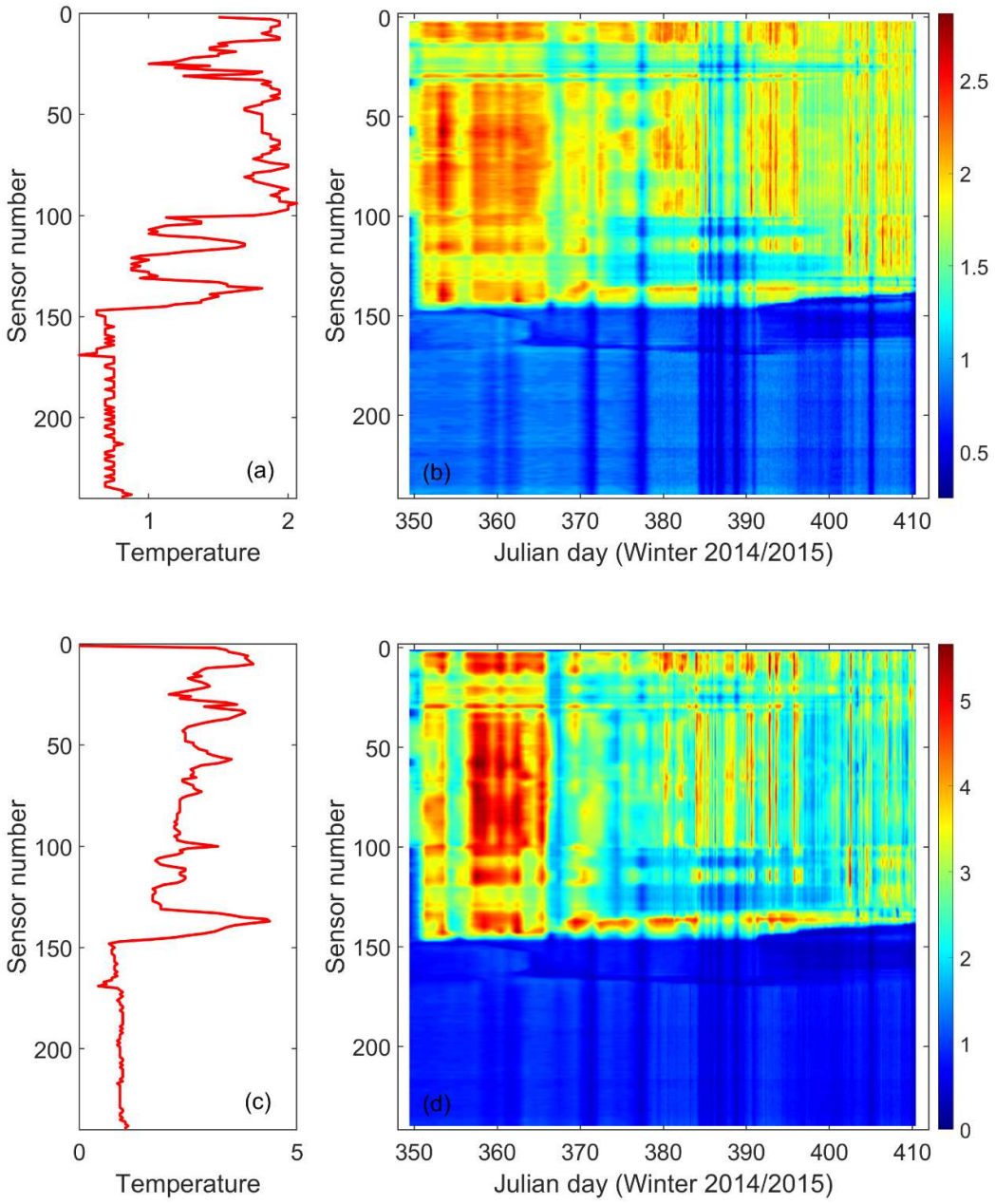

Figure 4. Illustrations of SIMBA-HT: a) a snapshot (25 January, 2015, 18:00 UTC) of vertical profile of observed temperature increase after 60 s., b) SIMBA-HT (60s) field observed by 240 sensors; c)

Same as a) but after heating for 90 s., and d) SIMBA-HT (90s) field observed by 240 sensors;

3.1.3 SIMBA snow depth and ice thickness

Snow depth and ice thickness are derived from SIMBA-ET and SIMBA-HT data. A common procedure is to look SIMBA-ET temperature profiles manually and identify sudden changes of vertical temperature gradient to locate the air-snow, snow-ice and ice-water interfaces. The snow depth is then calculated as the distance between the air-snow and snow-ice interfaces, and the ice thickness is the distance between the snow-ice and ice-water interfaces. However, a manual procedure is a heavy task, especially if SIMBA operation covers long period or one would need real time SIMBA results. Several studies have been carried out aiming development of an algorithm to obtain snow depth and ice thickness automatically (Liao et al., 2019, Zuo, et al., 2019, Cheng et al., 2020).

Below we present an example of the application of the Cheng et al, (2020) algorithm to retrieve snow depth and ice thickness from SIMBA data observed in Lake Orajärvi. When SIMBA was deployed, the initial sensor position at snow-ice interface is known and we defined it as Z_{gi0}, i.e. zero reference position for granular ice. During observation period, in case if initial snow-ice interface is moving upward from Z_{gi0}, which is a common phenomenon in Arctic lakes, the distance between Z_{gi0} and moving snow-ice interface is the new granular ice thickness formed by snow to ice transformation. The depth difference between total ice thickness and granular ice thickness is the congelation ice formed at the ice bottom. Figure 5 shows the air-snow, snow-ice and ice-water interfaces with SIMBA-ET (a) and SIMBA-HT (b) as the background. For better clarity, 5-day running average can be produced as the final products.

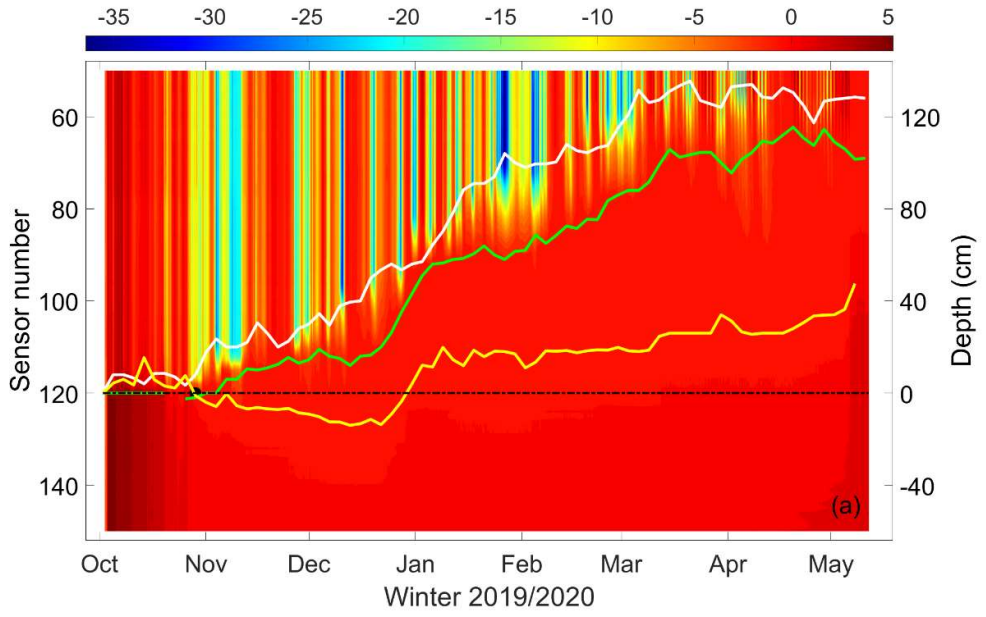

240

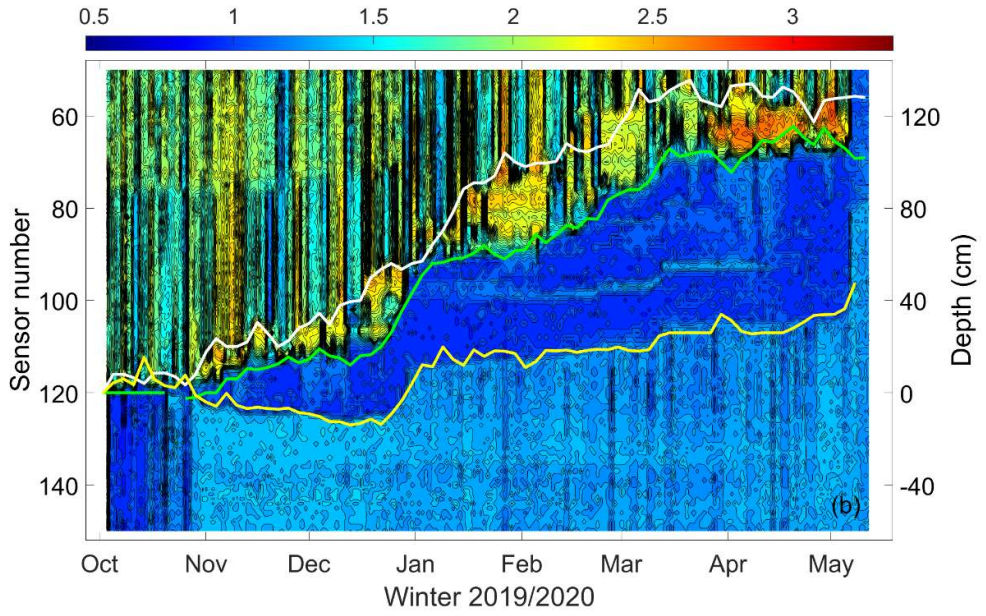

241

242 Figure 5. Time series of sensor position for the air-snow (white), snow-ice (green) and ice-water
243 (yellow) interfaces, identified applying the SIMBA algorithm. The SIMBA-ET observation is
244 illustrated as background in a), and SIMBA-HT ratio (HT60/HT90) in b). The black dash line shows
245 the sensor number (120) at the initial ice surface (Z_{gi0}). For clarity, we only illustrate sensors 50 –
246 150.

247

248 Using snow/ice interface as the zero-reference level, time series can be calculated for the snow depth,

snow-ice thickness, total ice thicknesses, and ice freeboard. Figure 6 is an example of the 2019/2020 time series, indicating that the lake ice was mainly granular ice, which was related to heavy snow fall during the ice season. The snow depth observed at FMI-ARC weather station on land was the highest in a decade. A few *in situ* observations (symbols in Fig. 6) were made during ice season. Point comparison between SIMBA algorithm detected and *in situ* observed values ranged from 2 centimeters up to 12 centimeters. The mean biases are 5, -1, 3 and 2 cm for snow depth, freeboard, granular and total ice thickness, respectively. Small values were largely due to the compensation effect. To validate algorithm, a lot more *in situ* observations are needed. Such analyses can be found in Cheng et al., (2020).

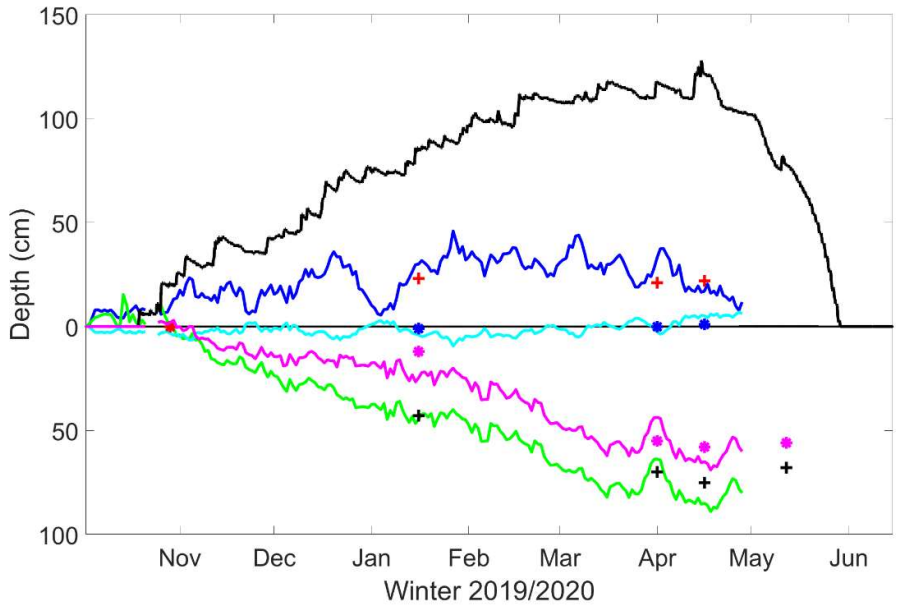

Figure 6. Products derived on the basis of SIMBA data: snow depth (blue), ice freeboard (cyan), granular ice thickness (magenta), and total ice thickness (green). The symbols represent *in situ* observations of snow depth (+), ice freeboard (●), granular ice thickness (●) and total ice thickness (+). The black solid line denotes the snow depth on land.

3.2 Weather data

The observed daily mean values of meteorological parameters for all seasons are presented in Figure 7. The inter-annual mean, maximum and minimum air temperatures are -2.5 ºC, -16.5 ºC and -5.5 ºC, respectively. The air temperature reveals a constant decreasing pattern from November to January. The coldest months are January and February. From March onward, the air temperature increased

gradually due to increasing solar radiation (Fig. 7c). The inter-annual average, maximum and minimum downward longwave radiative fluxes are 259 W/m^2, 309 W/m^2, and 201 W/m^2, respectively. The corresponding values for downward shortwave radiative fluxes are 64 W/m^2, 97 W/m^2, 26 W/m^2.

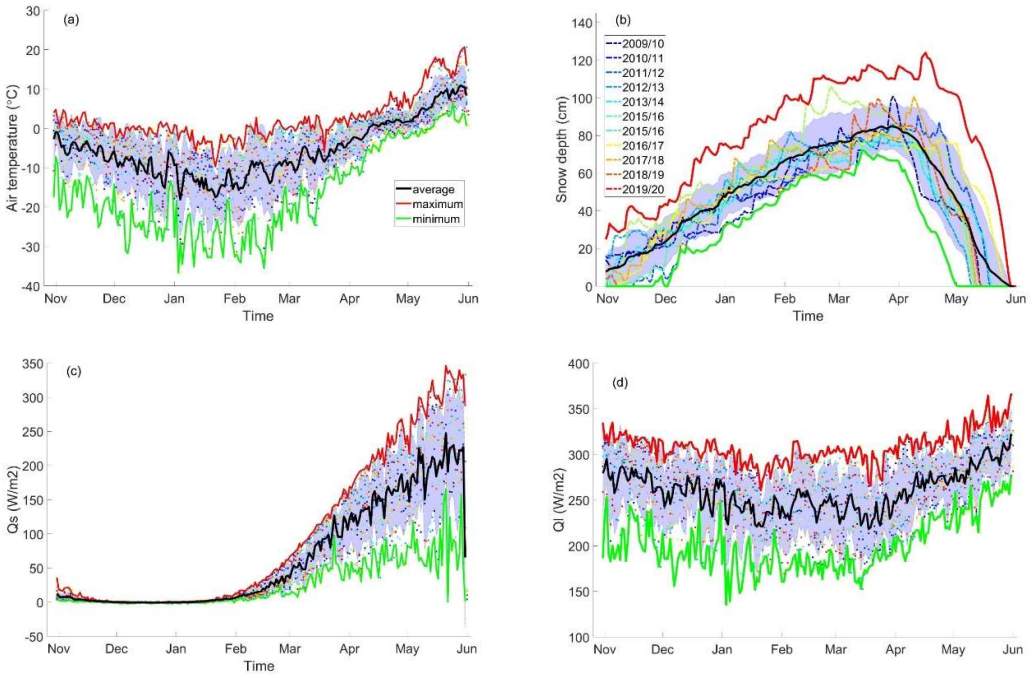

Figure 7. The observed (dots) daily mean air temperature (a), snow depth (b), downward shortwave (c), and longwave (d) radiative fluxes for each ice season between 1 November and 31 May. The solid lines represent decadal daily maximum (red), minimum(green) and average (black) values. The shadow area represents the standard deviation (STD). For snow depth, daily mean values are given as thin color lines.

Table 2 Summary of various meteorological and physical observations between 1 November and 31 May. For meteorological parameters (*Va*, *Ta, RH, cn, Qs, Ql*) the values are seasonal mean ± standard deviation.

Season	*Va* *m/s*	*Ta* *ºC*	*RH* *(%)*	*cn* *(-)*	*Qs* *W/m²*	*Ql* *W/m²*	*Tprec* *(mm)*	*Hsmax* *(cm)*	*AFDD* *ºC*	*ATDD* *ºC*
2009/2010	2.2±0.3	-6.8±9.4	84±9	0.7±0.1	62.9±76.8	267±31	201	101	-1717	304
2010/2011	2.2±0.6	-8±9.5	83±9	0.6±0.1	64.1±76.5	259±27	157	72	-1955	286
2011/2012	2.4±0.4	-5.1±7.2	84±11	0.7±0.1	64.4±82.3	264±21	272	91	-1308	239
2012/2013	2.2±0.2	-6.3±8.5	80±13	0.6±0.2	67±85.6	250±31	192	82	-1683	346

2013/2014	2.6±0.4	-4.6±6.4	81±10	0.7±0.1	61.6±81.8	261±19	267	81	-1214	243
2014/2015	2.7±0.6	-4.3±6.6	84±8	0.7±0.1	55.8±67.2	264±21	286	87	-1148	249
2015/2016	2.3±0.3	-4.2±8.4	84±10	0.7±0.1	61.5±81	265±25	287	106	-1261	354
2016/2017	2.8±0.3	-5.9±4.7	81±10	0.7±0.1	64.9±81.2	252±14	186	82	-1338	101
2017/2018	2.5±0.4	-6±8.7	80±12	0.7±0.2	66.5±82.7	256±27	219	101	-1615	362
2018/2019	2.7±0.4	-5.4±7.9	84±10	0.6±0.1	63.5±79.8	258±26	256	100	-1432	293
2019/2020	2.8±0.5	-5±5.1	84±13	0.6±0.1	70.1±92.9	258±13	285	124	-1242	188

Tprec: total accumulated precipitation in water equivalent (mm); Hsmax: the maximum observed snow depth on land. AFDD: The accumulated freezing degree day: the sum of daily mean air temperature below freezing point; ATDD: The accumulated thawing degree day: the sum of daily mean air temperature above freezing point.

Figure 7b clearly indicates that snow depth for the 2019/2020 season represented an extreme condition in a decade. There is an increasing trend of total precipitation during the ice season (Fig. 8). The total seasonal accumulated total precipitation is highly correlated (correlation coefficient r = 0.93) with the seasonal mean air temperature. The correlations between seasonal mean/maximum snow depth and corresponding air temperature are much lower r = 0.40 and r = 0.38, respectively. The correlation between total accumulated precipitation and maximum snow depth was 0.55. The difference is contributed by the snow drift and changes of snow metamorphism.

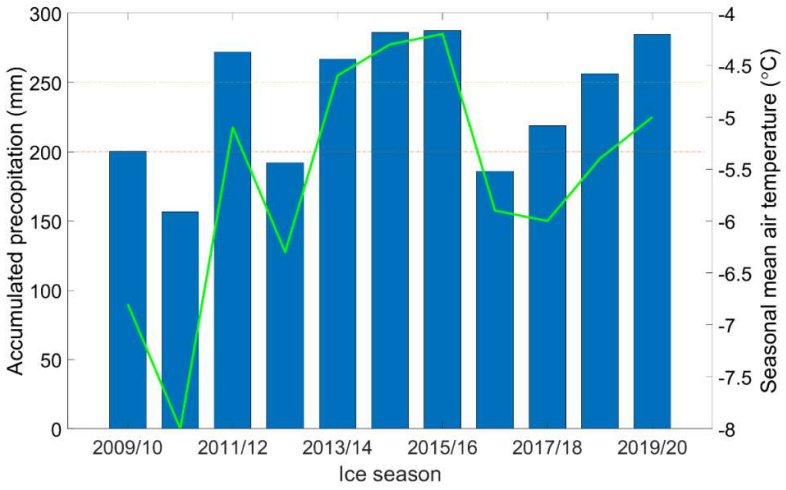

Figure 8. The accumulated total precipitation and mean air temperature between 1 November and 31 May.

4. Discussions

4.1 Inter-annual variation of SIMBA snow and ice products

Applying the SIMBA algorithm (Cheng et al., 2020), we obtained lake snow and ice products for all seasons (see data availability). Figure 9 shows the observed seasonal maximum values for the snow depth, maximum total ice thickness, and maximum granular ice thickness. During the observation period, both snow depth and ice thickness showed increasing trends. The increase of granular ice thickness is the fastest among all the snow and ice components. It reached the maximum 80% of the total ice thickness in 2019/2020. In Lake Orajärvi, snow mass has contributed to the ice thickness during every winter season. The maximum granular ice thickness was on average about 40% of the maximum total ice thickness during the data period. For all seasons, the correlation coefficient between the maximum granular ice thickness and the maximum ice thickness was 0.64. The occurrence of maximum lake snow is, on the average, about one month prior to the maximum granular ice formation (Fig. 10). Because of snow to ice transformation, the time series of snow depth in the lake is not correlated with the snow depth on land. The snow depth on lake ice ranged from 25 to 43% of that on land. On the average the ratio was 0.33, some 11% less than observed for a lake in southern Finland (Kärkäs, 2000). In several seasons, when SIMBA were recovered in late April or early May, the entire snow layer on lake ice was transferred to granular ice. Granular ice reached its maximum value when the ice surface was free of snow.

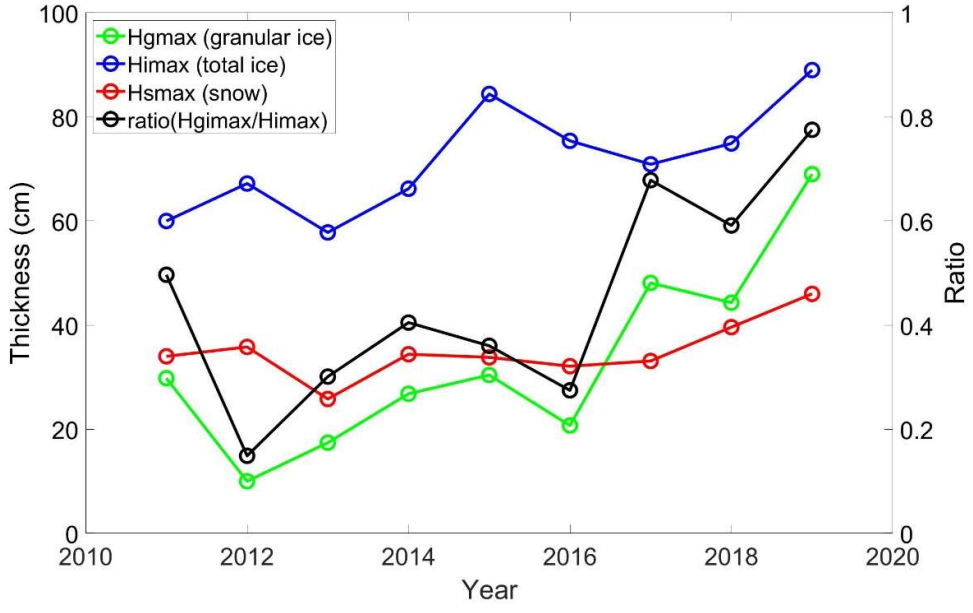

Figure 9. SIMBA observed seasonal maximum snow depth (red), maximum total ice thickness (blue), maximum granular ice thickness (green) and the ratio between granular ice and total ice thickness (black) during observation seasons.

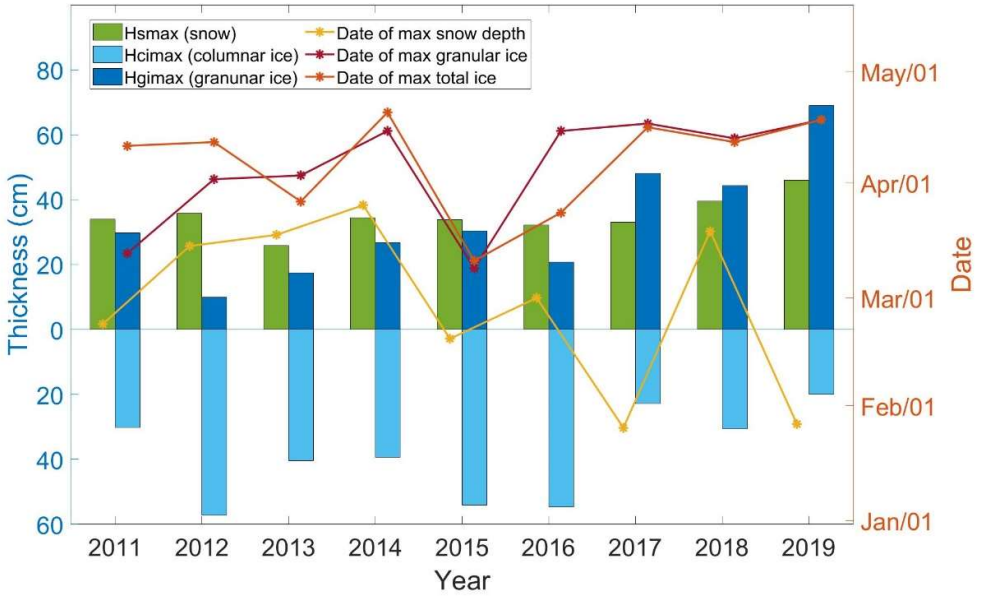

Figure 10. Seasonal maximum snow depth, granular ice thicknesses, congelation ice thicknesses, and the date when those values were observed.

4.2 Inter-annual variation of temperature conditions

According to weather observations in Sodankylä, the air temperature increased by about 0.16 ºC/year during the last deacde. For the period from 1980 – 2020, the air temperature has an increasing trend of about 0.06 ºC/year. On the average, the increase of air temperature in last decade is about 3 times faster than the past 40 years in agreement with the findings of Przybylak and Wyszyński (2020) for the high Arctic. The accumulated precipitation correlated better to the maximum snow depth on land ($r = 0.55$) than the mean snow depth ($r = 0.45$). It is, however, not correlated ($r = 0.21$) with snow depth on the lake ice.

The seasonal AFDD and ATDD for each winter season are shown in Figure 11. A negative decreasing of AFDD was seen in response to the increase of air temperature. AFDD is directly linked with thermodynamic ice formation. During a given period, a decrease of AFDD is expected to result in less formation of columnar ice. However, during our observation period, the total ice thickness revealed an increasing trend. The increase of ice thickness is due to snow-ice formation. The trend of

ATDD is very insignificant, suggesting that the melting of lake ice due to temperature increase has not increased much during the observation decade.

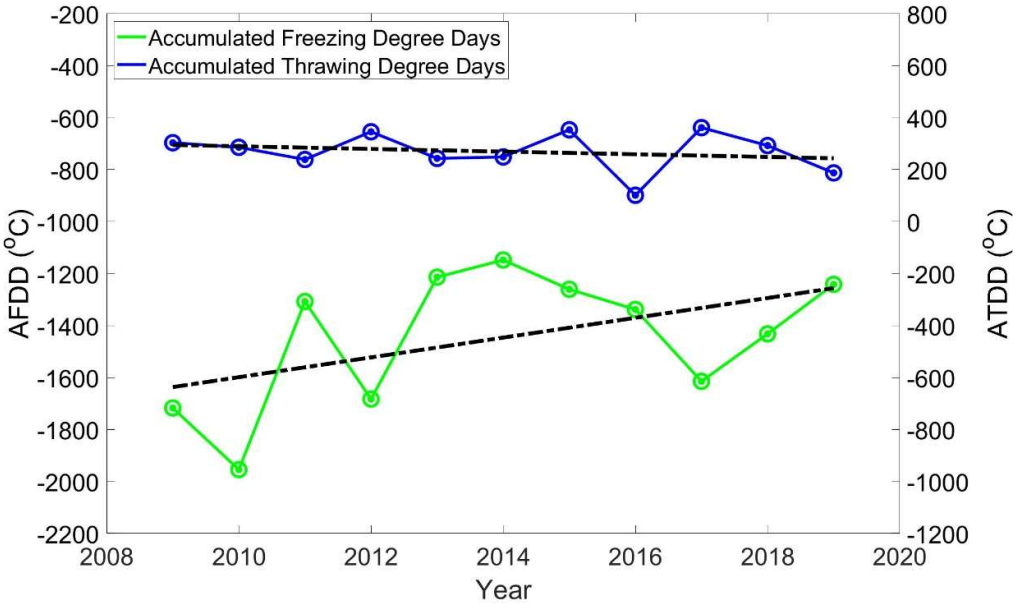

Figure 11. The seasonal accumulated freezing degree day (AFDD) and thaw degree day (ATDD) during the observation period (2009/2010 – 2019/2020).

4.3 Challenges of the SIMBA program

SIMBA observations in Lake Orajärvi represent a small but sustainable program, so far ran for a decade. A few times we have encountered malfunction of SIMBA, especially in the early phases of the SIMBA program. In recent years, SIMBA has become more robust without need for heavy-duty maintenances during field measurements, and the system has been remarkably improved with respect to the quality of HT measurements. Several snow and ice products can be derived from SIMBA's two type of temperature (SIMBA-ET and SIMBA-HT) measurements. The SIMBA program has largely benefited from the Sodankylä supersite infrastructure, where the comprehensive and high standard meteorological observations are available.

Challenges remain in further improvement of the SIMBA program. Due to safety issues, SIMBA must be deployed and recovered when ice is strong enough. Hence, the early freeze-up and late break-up cannot be monitored. In Autumn 2019, a wooden floating raft was deployed and anchored in Lake Orajärvi. SIMBA was, for the first time, deployed during ice-free season on 1 October. This kind of deployment will be carried out also in the future, allowing year-round SIMBA measurements.

Part of the thermistor chain exposed in the air above the snow surface may suffer from frost in winter or from solar heating in spring, and also the sensors in the upper layers of snow and ice may suffer from solar heating, resulting in large uncertainties in SIMBA-ET and SIMBA-HT readings. To compensate the effect of temperature errors on snow depth detection, one solution is to deploy Acoustic Rangefinder Sounders (ARS) to measure the evolution of snow surface. In fact, an ARS has been deployed in the past two winter seasons. These data sets can also be used to understand the effect of wind on snow drift and quantify snow surface sublimation in winter.

During the melting season, both SIMBA-ET and SIMBA-HT strongly raise in the upper part of the ice resulting an isothermal status of the entire ice column. In this condition, SIMBA snow depth and ice thickness values are liable to large errors. Combination of SIMBA observations and numerical model experiments may yield more reliable results in such conditions.

SIMBA measurements have been taken automatically, but it is still important to carry out *in situ* observations, such as collecting ice core and snow samples, as such observations cannot be made by automatic instruments.

4 Data availability

The data are archived at https://zenodo.org/record/4559368#.YEIYOtyxVPZ (Cheng et al., 2021). The 4 zip-files should be unzipped in different file folders preferably using zip-file names as the folder names. A readme file exists in each folder. The *in situ* snow depth and ice thickness observations for 2009/2010 - 2012/2013 as well as a description file of SIMBA deployment and recovery for each ice season (SIMBA_D&R_all_Years.docx) are provided.

5 Conclusions

A thermistor string-based snow and ice mass balance apparatus (SIMBA) has been deployed in an Arctic lake since 2009. The measurements covered most part of the ice season from mid-December to late April/early May. SIMBA-ET and SIMBA-HT temperature observations are described in this paper. The daily snow depth and ice thickness were derived from SIMBA temperature field applying a validated automatic algorithm (Cheng et al., 2020). The meteorological parameters for winter seasons (1 November - 31 May) are also collected and discussed. During the investigation decade, the air temperature in the ice season has had an increasing trend of 0.16 ºC/year. The warming rate is

388 comparable to the result find for the high Arctic by Przybylak and Wyszyński (2020). The increase of
389 air temperature in winter season is highly correlated (0.93) with seasonal total accumulated
390 precipitation. This is because warm winters in the study region are also wet and characterized by a
391 high cyclone activity. Transient cyclones are vital for the transport of warm, moist air masses to
392 Northern Europe (Wickström et al., 2020). The precipitation in season 2019/2020 represented an
393 extreme episode during the study decade. Despite of the air temperature increase, the total maximum
394 ice thickness in the lake has an increasing trend. The increase of maximum ice thickness is due to the
395 increase of granular ice. The interannual variability of maximum granular ice thickness is large
396 ranging from 15 to 80% of the total maximum ice thickness. The time series of the SIMBA ET and
397 HT allow identification of moving air-snow, snow-ice and ice-water interfaces. Because of the air
398 temperature increase, the seasonal AFDD reduces. This results in a decreasing impact of below-zero
399 air temperatures on lake ice growth during the freezing season, as the growth of columnar ice is
400 reduced. Simultaneously, the role of precipitation on total ice formation is enhanced because snow-
401 ice and superimposed ice contribute to an increasing fraction of the total ice thickness. The trend in
402 ATDD was negligible, suggesting that the effect of air temperature on ice melting has remained
403 unchanged.

404 To our knowledge, this is the first decadal-scale SIMBA data set ever collected from an Arctic Lake.
405 The data provides information on snow and ice mass balance and the controlling atmospheric factors.
406 The measurements will continue in the future.
407 The weather observations, e.g., decadal time series of daily maximum and minimum weather
408 parameters, can be used to estimate snow and ice conditions in the lake applying a snow/ice model
409 (e.g., Cheng et al., 2014). The SIMBA data are not only suitable for snow/ice surface heat and mass
410 balance studies. The temperatures at the ice bottom and in the water below are valuable to understand
411 the lake thermal structure and water-ice heat transfer (Huang et al., 2019b).
412 The SIMBA program, with Lake Orajärvi as a testbed, offers excellent opportunities for
413 dissemination of cryospheric knowledge and related outreach, providing rich possibilities for
414 community collaborations both nationally and internationally. The observed changes in snow depth
415 and composition of lake ice contribute to better understanding of cryospheric aspects of climate
416 change. For example, parameterizations of the discovered snow and ice processes can be improved
417 in climate models.

Snow and ice measurements similar to those in Lake Orajärvi have been recently initiated in Wulaingsuhai lake in an arid climate zone in Inner-Mongolia of China. The observations focused on lake ice mass balance (Lu et al., 2020) and energy budget, in particular the solar radiation (Cao et al., 2020). In a long run, the corresponding lake snow and ice measurements at both sites and possible similar observations in a thermokarst lake (e.g., Huang et al, 2019a, 2019b) at Qinghai-Tibet Plateau, often referred to as the "Third Pole of the Earth" can be used together to carry out coordinated research.

Author contributions

BC and TV initiated the SIMBA program, draft the manuscript; YC, BC, FZ and YQ developed the SIMBA algorithm processed the SIMBA data and analyses the results; JP, AK and JL are responsible for supersite and various meteorological *in situ* observations and data collections. All authors contributed for writing the manuscript.

Competing interests

The authors declare no competing interests.

Acknowledgement

We are grateful to Mr. Pekka Kosloff for carrying out fieldwork in Lake Orajärvi for all the winter seasons. The logistical assistance provided by Mr. Jyrki Mattanen in FMI-ARC, Sodankylä are acknowledged. The study was for financial support by FMI long-term sustainable SIMBA program. The data analyses were partly supported by the European Union's Horizon 2020 research and innovation programme [727890 – INTAROS]; Academy of Finland under contract 317999, and the National Key Research and Development Program of China (No. 2017YFE0111700 – MARIS). We thank comments from Dr. Keith Jackson, one anonymous reviewer and topical editor Dr. Xin Li that helped to improve the manuscript.

References

Anderson, E.J., Fujisaki-Manome, A., Kessler, J., Lang, G.A., Chu,P. Y., Kelley, J.G.W., Chen, Y., and Wang, J.: Ice Forecasting in the Next-Generation Great Lakes Operational Forecast System (GLOFS), J . Mar. Sci. Eng., 6, 123; doi:10.3390/jmse6040123, 2018.

448 Ballinger, T.J., Overland, J.W., Wang, M., Bhatt, U.S., Hanna, E., Hanssen-Bauer, I., Kim, S.-J.,
449 Thoman, R.L., and Walsh, J.E.: Surface air temperature, Arctic Report Card, DOI: 10.25923/gcw8-
450 2z06, 2020.
451 Bintanja, R.: The impact of Arctic warming on increased rainfall, Scientific Report.
452 DOI:10.1038/s41598-018-34450-3, 2018.
453 Box, J.E. and 19 others: Key indicators of Arctic climate change: 1971–2017, Environ. Res. Lett. 14
454 045010, 2019.
455 Brown, L. C. and Duguay, C.R.: The response and role of ice cover in lake climate interactions.
456 Progress in Physical Geography: Earth and Environment 34(5), 671–704, 2010.
457 Cheng, B., Vihma T., Rontu, L., Kontu, A. Kheyrollah Pour H., Duguay C. and Pulliainen, J.:
458 Evolution of snow and ice temperature, thickness and energy balance in Lake Orajärvi, northern
459 Finland, Tellus A: Dynamic Meteorology and Oceanography 66(1), 21564, 2014.
460 Cheng, Y., Cheng, B., Zheng, F., Vihma, T., Kontu, A., Yang, Q. and Liao, Z.: Air/snow, snow/ice and
461 ice/water interfaces detection from high-resolution vertical temperature profiles measured by ice
462 mass-balance buoys on an Arctic lake, Annals of Glaciology 1–11. https://doi.org/10.1017/
463 aog.2020.51, 2020
464 Cheng, B., Cheng, Y., Vihma, T., Kontu, A., Zheng,F., Lemmetyinen, J., and Pulliainen, J.: SIMBA
465 snow/ice mass balance buoy data and weather station data[Data set]. Earth System Science Data
466 (ESSD). Zenodo. http://doi.org/10.5281/zenodo.4559368, 2021.
467 Cao, X., Lu, P., Leppäranta, M., Arvola, L., Huotari, J., Shi, X., Li, G., and Li, Z.: Solar radiation
468 transfer for an ice-covered lake in the central Asian arid climate zone. Inland Waters,
469 doi:10.1080/20442041.2020.1790274, 2020.
470 Filazzola, A., Brown, C., Dettlaff, M.A., Batbaatar, A., Grenke, J., Bao, T., Heida, I.P., and Cahill
471 Jr, J.F.: The effects of livestock grazing on biodiversity are multitrophic: a meta-analysis, Ecology
472 Letters, 23: 1298–1309, https://publons.com/publon/10.1111/ele.13527, 2020.
473 Hoppmann, M., Nicolaus, M., Hunkeler, P. A., Heil,H., Behrens, L.-K. Konig-Langlo, G., and Gerdes,
474 R.: Seasonal evolution of an ice-shelf influenced fast-ice regime, derived from an autonomous
475 thermistor chain, J. Geophys. Res. Oceans, 120, 1703– 1724, doi:10.1002/2014JC010327, 2015.
476 Huang, W., Cheng, B., Zhang, J., Zhang, Z., Vihma, T., Li, Z., and Niu, F.: Modeling experiments on
477 seasonal lake ice mass and energy balance in the Qinghai–Tibet Plateau: a case study, Hydrol. Earth

478 Syst. Sci., 23, 2173-2186, https://doi.org/10.5194/hess-23-2173-2019, 2019a.
479 Huang, W., Zhang, J., Leppäranta, M., Li, Z., Cheng, B. and Lin, Z.: Thermal structure and water-ice
480 heat transfer in a shallow ice–covered thermokarst lake in central Qinghai-Tibet Plateau. Journal of
481 Hydrology, 578, [124122]. https://doi.org/10.1016/j.jhydrol.2019.124122, 2019b
482 Jackson, K., Wilkinson, J., Maksym, T., Meldrum, D., Beckers, J., Haas, C., and Mackenzie, D.: A
483 novel and low-cost sea ice mass balance 1010 buoy. J. Atmos. Ocean. Tech. 30(11), 2676-2688. DOI:
484 10.1175/JTECH-D-13-00058.1., 2013
485 Kang, K.-K., Duguay, C.R., Lemmetyinen, J., and Gel, Y.: Estimation of ice thickness on large
486 northern lakes from AMSR-E brightness temperature measurements. Remote Sensing of
487 Environment 150, 1–19, doi: 10.1016/j.rse.2014.04.016, 2014.
488 Kärkäs, E-: The ice season of Lake Pääjärvi in southern Finland. Geophysical Research Letters 36(1–
489 2), 85–94, 2000.
490 Lei, R., Cheng, B., Heil, P., Vihma, T., Wang, J., Ji, Q., and Zhang, Z.: Seasonal and interannual
491 variations of sea ice mass balance from the central Arctic to the Greenland Sea. Journal of
492 Geophysical Research: Oceans 123(4), 2422–2439, 2018.
493 Lei, R., Hoppmann, M., Cheng, B., Zuo, G., Gui, D., Cai, Q., Belter, H. J., and Yang, W.: Seasonal
494 changes in sea ice kinematics and deformation in the Pacific sector of the Arctic Ocean in 2018/19,
495 The Cryosphere, 15, 1321–1341, https://doi.org/10.5194/tc-15-1321-2021, 2021.
496 Leppäranta, M.: Modelling the formation and decay of lake Ice. In George G (ed.), The Impact of
497 Climate Change on European Lakes. Dordrecht, Netherlands: Springer, pp. 63–83, 2010.
498 Leppäranta, M.: Freezing of Lakes and the Evolution of Their Ice Cover. Berlin Heidelberg: Springer,
499 2015.
500 Liao, Z., Cheng, B., Zhao, J., Vihma, T., Jackson, K., Yang, Q., Yang, Y., Zhang, L., Li, Z. Qiu, Y. and
501 Cheng, X.: Snow depth and ice thickness derived from SIMBA ice mass balance buoy data using an
502 automated algorithm. International Journal of Digital Earth 12(8), 962–979, 2019.
503 Lu, P., Cao, X., Li, G., Huang, W., Leppäranta, M., Arvola, L., Huotari, J., and Li, Z.: Mass and heat
504 balance of a lake ice cover in the central Asian arid climate zone. Water, 12(10), 2888,
505 doi:10.3390/w12102888, 2020.
506 Mermoz, S., Allain-Bailhache, S., Bernier, M., Pottier, E., Sanden, J. J. Van Der, and Chokman. K.:
507 Retrieval of river ice thickness from C-band PolSAR data. IEEE Transactions on Geoscience and

508 Remote Sensing 99, 1–11, doi: 10.1109/TGRS.2013.2269014, 2013.
509 Provost, C., Sennechael, N., Miguet, J., Itkin, P., Rosel, A., Koenig, Z., Villacieros-Robineau, N., and
510 Granskog. M.A.: Observations of flooding and snow-ice formation in a thinner Arctic sea-ice regime
511 during the N-ICE2015 campaign: influence of basal ice melt and storms. Journal of Geophysical
512 Research: Oceans 122(9), 7115–7134, doi:10.1002/2016JC012011, 2017.
513 Przybylak R, Wyszyński P.: Air temperature changes in the Arctic in the period 1951– 2015 in the
514 light of observational and reanalysis data. Theor. Appl. Climatol. 139: (1–2):75–94.
515 DOI: 10.1007/s00704-019-02952-3, 2020
516 Richter-Menge JA, Perovich DK, Elder BC and Claffey K: Ice mass balance buoys: a tool for
517 measuring and attributing changes in the thickness of the Arctic sea-ice cover. Annals of Glaciology
518 44, 205–210. 2006
519 Sharma, S., Blagrave, K., Magnuson, J.J., M. O'Reilly, C., Oliver, S., D. Batt, R., R. Magee, M.,
520 Straile,D., Weyhenmeyer, G.A. Winslow, L., Woolway, R.I.: Widespread loss of lake ice around the
521 Northern Hemisphere in a warming world. Nat. Clim. Chang. 9, 227–231.
522 https://doi.org/10.1038/s41558-018-0393-5, 2019.
523 Tikkanen, M.: Climate. In: The Physical Geography of Fennoscandia (ed. M. Seppälä). Oxford:
524 Oxford University Press, pp. 96112, 2005.
525 Wei L., Deng X., Cheng B., Vihma T., Hannula H., Qin T., and Pulliainen J.: The impact of
526 meteorological conditions on snow and ice thickness in an Arctic lake. Tellus - Series A: Dynamic
527 Meteorology and Oceanography, Vol 68: 1~12, 2016.
528 Wickström, S., Jonassen, M., Vihma, T, and Uotila, P.: Trends in cyclones in the high latitude North
529 Atlantic during 1979-2016. Q. J. R. Meteorol. Soc.,146, 762–779, DOI: 10.1002/qj.3707, 2020.
530 Woolway, R., Weyhenmeyer, G.A., Schmid, Dokulil, M.T., de Eyto, E., Maberly, S.C., May, L., and
531 Merchant, C. J.: Substantial increase in minimum lake surface temperatures under climate change.
532 Climatic Change 155, 81–94. https://doi.org/10.1007/s10584-019-02465-y, 2019.
533 Wu, Y., Duguay, C, R, and Xu, L.: Assessment of machine learning classifiers for global lake ice
534 cover mapping from MODIS TOA reflectance data, Remote Sensing of Environment, Vol 253,
535 112206 https://doi.org/10.1016/j.rse.2020.112206, 2021.
536 Zuo, G., Dou, Y., Lei, R.: Discrimination algorithm and procedure of snow depth and sea ice thickness
537 determination using measurements of the vertical ice temperature profile by the ice-tethered buoys.

Sensors 18, 4162. https://doi.org/10.3390/s1812416, 2018.